

Optimization of growth conditions for InGaAs/InAlAs/InP quantum cascade lasers by metalorganic chemical vapor deposition

Yong Huang^a, Jae-Hyun Ryou^{a,*}, Russell D. Dupuis^{a,b}, Christian Pflügl^c, Federico Capasso^c, Kewei Sun^d, Alec M. Fischer^d, Fernando A. Ponce^d

^a Center for Compound Semiconductors and School of Electrical and Computer Engineering, Georgia Institute of Technology, 777 Atlantic Dr. NW, Atlanta, GA 30332-0250, USA

^b School of Materials Science and Engineering, Georgia Institute of Technology, Atlanta, GA 30332, USA

^c School of Engineering and Applied Sciences, Harvard University, 19 Oxford Street, Cambridge, MA 02138, USA

^d Department of Physics, Arizona State University, Tempe, AZ 85287-1504, USA

ARTICLE INFO

Article history:

Received 1 October 2010

Received in revised form

9 December 2010

Accepted 13 December 2010

Communicated by R.M. Biefeld

Available online 17 December 2010

Keywords:

A1. Characterization

A3. Metalorganic chemical vapor deposition

B2. Semiconducting III–V materials

B3. Infrared devices

B3. Laser diodes

ABSTRACT

We investigate the growth conditions for lattice-matched InGaAs/InAlAs/InP quantum cascade lasers (QCLs) by metalorganic chemical vapor deposition (MOCVD). Effect of substrate misorientation, growth temperature, and V/III ratios of InGaAs and InAlAs layers on the surface morphology, optical quality, and impurity incorporation were systematically studied. It was found that epitaxial layers and multi-quantum-well structures grown at 720 °C with V/III ratios of 116 for InGaAs and 21 for InAlAs on InP substrates with an off-cut angle of $\sim 0.06^\circ$ exhibit a stable step-flow growth and low oxygen and carbon contamination. Using these conditions, a $\sim 11.3\text{-}\mu\text{m}$ -thick QCL with an emission wavelength at $\sim 9.2\ \mu\text{m}$ was grown and fabricated, which demonstrated excellent structural quality and operated at room temperature in pulsed mode with a threshold current density of $2.0\ \text{kA}/\text{cm}^2$ and a slope efficiency of $550\ \text{mW}/\text{A}$.

© 2010 Elsevier B.V. All rights reserved.

1. Introduction

Quantum cascade lasers (QCLs) are unipolar light emitting devices based on resonant tunneling and intersubband transitions in a multiple-quantum well (MQW) or superlattice (SL) structure [1]. The emission wavelength of QCLs covers the mid- and long-infrared region from $\lambda=2.6$ to $\lambda=25\ \mu\text{m}$ and part of the terahertz region of the spectrum [2,3], which opens up many immediate or potential applications in chemical and biological sensing, spectroscopy, astronomy and medical imaging. While tremendous progress has been made in improving the device performance via QCL structure design since its first demonstration in 1994 [4–13], there are few studies on the epitaxial growth itself [14–17], which, indeed, represents one of the most challenging tasks for semiconductor material growers. The QCL structure, with total thickness easily exceeding $10\ \mu\text{m}$ and number of layers close to thousand, requires a precise control over the composition, thickness, background doping, and interface abruptness of each layer. This is one of the reasons that molecular beam epitaxy (MBE) was the only growth method for creating QCLs during their first 10 years of investigation. The demonstration of QCLs grown by

metalorganic chemical vapor deposition (MOCVD) in 2003 [18], however, provides a growth technique for these devices which is more suited to mass-production with device performance comparable to MBE-grown QCLs through progressive improvements [19].

In this work, we systematically studied the MOCVD growth conditions for lattice-matched InGaAs/InAlAs/InP heterostructures and QCLs. We show how the key growth parameters such as substrate misorientation, growth temperature, and V/III ratios of InGaAs and InAlAs layers can be chosen to achieve a stable step-flow growth mode. Using the optimized growth condition, a QCL with an emission wavelength at $\sim 9.2\ \mu\text{m}$ was grown and fabricated, which operates at room temperature with a peak power of $480\ \text{mW}$ and a slope efficiency of $550\ \text{mW}/\text{A}$.

2. Experimental procedure

Epitaxial growth of $\text{In}_{0.53}\text{Ga}_{0.47}\text{As}/\text{In}_{0.52}\text{Al}_{0.48}\text{As}/\text{InP}$ SL structures and QCLs was carried out by MOCVD in a Thomas Swan $7 \times 2''$ reactor system equipped with a close-coupled showerhead growth chamber. EpipureTM trimethylindium (TMIn, $\text{In}(\text{CH}_3)_3$), trimethylgallium (TMGa, $\text{Ga}(\text{CH}_3)_3$), trimethylaluminum (TMAI, $\text{Al}(\text{CH}_3)_3$), and triethylgallium (TEGa, $\text{Ga}(\text{C}_2\text{H}_5)_3$) were used as column III precursors [20] and arsine (AsH_3) and phosphine (PH_3) were used as column V precursors. The *n*-type dopant precursor was diluted

* Corresponding author. Tel.: +1 404 385 2403; fax: +1 404 385 6167.
E-mail address: jaehyun.ryou@gatech.edu (J.-H. Ryou).

disilane (Si_2H_6) balanced in hydrogen (H_2). The substrate used in the study was *n*-type (1 0 0) InP with different misorientations having tilt angles from 0.02° to 0.25° towards (0 1 $\bar{1}$). The epitaxial growth was performed at temperatures of $T_g=680\sim 740^\circ\text{C}$ at a reactor chamber pressure of 100 Torr. For material characterizations, the Nomarski optical microscopy, atomic-force microscopy (AFM), X-ray diffraction (XRD), transmission electron microscopy (TEM), photoluminescence (PL), and secondary-ion mass spectrometry (SIMS) were used to characterize the morphological, structural, optical properties, and the chemical analysis of the epitaxial layers.

QCL epitaxial structure was fabricated into ridge waveguides using standard optical lithography and wet etching processes. After forming the metal contacts by depositing Ti/Au stacks on the top and bottom of the wafer, the laser diode (LD) bars were cleaved and the cleaved facets were left uncoated. The substrate side was then alloyed onto a Cu heat sink and wire bonded. The devices were tested in pulsed mode at 80 kHz with 1% duty ratio at room temperature.

3. Results and discussion

InP-based QCL structures typically consist of multi-stage InGaAs/InAlAs SL active regions sandwiched by InGaAs waveguides and thick InP cladding layers. In such long growth runs to produce very thick epitaxial structures, the surface morphology and interface abruptness of the epitaxial layer structure can be strongly affected by the substrate surface quality and orientations, and the surface texture of the layers during growth, which makes

the material quality of the epitaxial structure very sensitive to the choice of substrate and the growth conditions. The crystalline defects and surface features that can be considered negligible (mainly due to low density and small feature size) become not negligible for the thick epitaxial layer growth. To find the optimal process condition window for QCL epitaxial growth, we rely on the calibration and assessment of thick layers. In the following, some key growth parameters are evaluated including substrate misorientation, growth temperature, and V/III ratio.

3.1. Effect of substrate misorientation on InGaAs and InP layers

Fig. 1 shows the microscopic surface morphology of unintentionally doped $\text{In}_{0.53}\text{Ga}_{0.47}\text{As}$ and InP layers grown at 700°C on InP substrates with different off-cut angles with respect to the (1 0 0) plane. The layer thickness is $\sim 2\ \mu\text{m}$ for InGaAs layer and $\sim 4\ \mu\text{m}$ for InP layer. As shown in Fig. 1(a)–(c), the InGaAs growth undergoes a step-flow mode regardless of the substrate misorientation employed in this study. Consequently, the actual off-cut angles can be estimated from the AFM images by measuring the average terrace width. However, the surface of InP layer has different features depending on the substrate misorientation. At a small off-cut angle of 0.02° in Fig. 1(d), the surface is very rough characterized by high-density hillocks. At a relatively large off-cut angle of 0.25° in Fig. 1(f), a step-bunched surface is observed. Only at an off-cut angle of 0.06° , the InP growth develops a step-flow mode as shown in Fig. 1(e). Since the hillocks appear when the surface step density is too low while the step-bunching occurs when the step density is too high, there should be an optimal off-cut angle for establishing a stable step-flow growth mode. In the case of InP

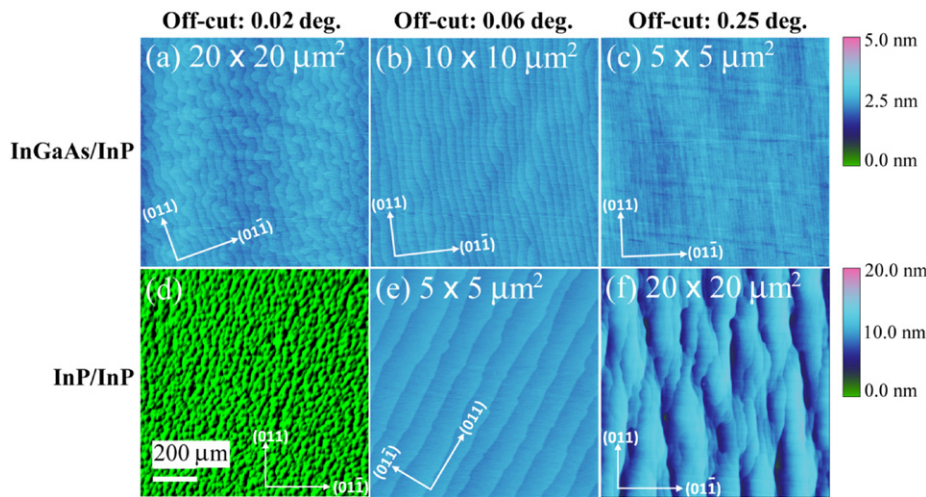


Fig. 1. Surface morphology of $\text{In}_{0.53}\text{Ga}_{0.47}\text{As}$ (the first row) and InP (the second row) on InP substrates with different off-cut angles: (a)–(c), (e), and (f) are microscopic images measured by AFM and (d) is the Nomarski optical micrograph. For the AFM images, the height scale for (a)–(c), and (e) is 5 nm and one for (f) is 20 nm. The surface orientation is labeled and the color bars for 5 and 20 nm are displayed. (For interpretation of the references to color in this figure legend, the reader is referred to the web version of this article.)

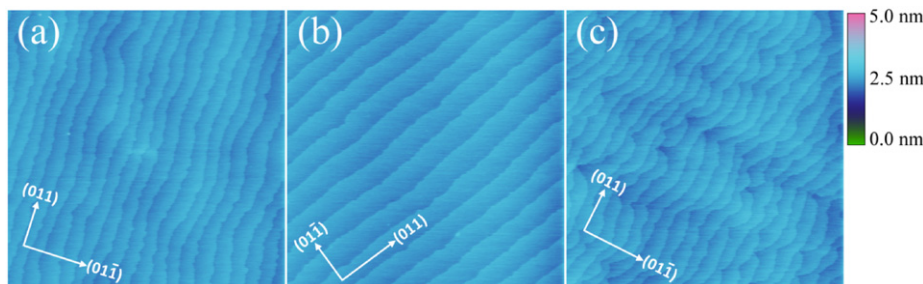


Fig. 2. AFM images ($10 \times 10\ \mu\text{m}^2$) of 30-period of $\text{In}_{0.53}\text{Ga}_{0.47}\text{As}/\text{In}_{0.52}\text{Al}_{0.48}\text{As}$ (8/15 nm) MQWs grown at (a) 680°C , (b) 720°C , and (c) 760°C . The height scale is 5 nm for all images.

layer under the growth condition in this study, the optimal angle is found to be between 0.05° and 0.1° . Although hillocks or step-bunching can be mitigated to some degree by changing the growth conditions such as growth rate and temperature [21,22], the most effective approach is to use the substrates with an optimized misorientation. Similar trends have been found in evaluating the optical quality of InGaAs/InAlAs QWs and morphology of InP and InAlAs on InP substrates [23,24]. Different device performance characteristics have also been reported for QCLs grown on GaAs substrates with different misorientations [25]. In the following studies, all the InP substrates used are with optimal misorientations with $0.07^\circ \pm 0.02^\circ$ off-cuts from (1 0 0).

3.2. Effect of growth temperature of SL structure

As the core of the active region of a QCL consists of $\text{In}_{0.53}\text{Ga}_{0.47}\text{As}/\text{In}_{0.52}\text{Al}_{0.48}\text{As}$ SLs, a high growth temperature is generally required to reduce oxygen (O) and carbon (C) impurities in the epitaxial layers as well as to enhance the surface mobility of aluminum (Al) adatoms in Al-containing layers [26]; however, too high growth temperature also deteriorates the optical and structural quality of InGaAs layers. Using different growth temperatures for InGaAs and InAlAs in the QCL structure is not practical in terms of growth time and interface quality of SL structures. Thus, an optimal window for $\text{In}_{0.53}\text{Ga}_{0.47}\text{As}/\text{In}_{0.52}\text{Al}_{0.48}\text{As}$ SL growth has to be found. Fig. 2 shows the AFM images of 30-period of $\text{In}_{0.53}\text{Ga}_{0.47}\text{As}/\text{In}_{0.52}\text{Al}_{0.48}\text{As}$ (8/15 nm) lattice-matched (to InP) MQWs grown at 680, 720, and 760 °C, respectively. Nominal input V/III ratios are 116 and 21 for $\text{In}_{0.53}\text{Ga}_{0.47}\text{As}$ and $\text{In}_{0.52}\text{Al}_{0.48}\text{As}$, respectively. Growth rate is ~ 0.15 nm/s for both materials. A stable step-flow growth was obtained only at 720 °C, which is characterized

by straight steps and constant terraces width, while irregular terraces and steps were observed at 680 and 760 °C. PL spectra were obtained for these MQW structures (not shown here). The full width at half maximum (FWHM) of the PL peak is also minimal for the MQWs grown at 720 °C, indicating the lowest well-width fluctuation, which is consistent with the AFM morphology.

To investigate the impurity concentration in the layers, the following test structure was grown: starting from the InP substrate, $\text{In}_{0.52}\text{Al}_{0.48}\text{As}$ (500 nm), $\text{In}(\text{Al}_{0.6}\text{Ga}_{0.4})\text{As}$ (Al mole fraction with respect to Ga in quaternary alloys: Q 60%, 150 nm), $\text{In}(\text{Al}_{0.25}\text{Ga}_{0.75})\text{As}$ (Q 25%, 150 nm), and $\text{In}_{0.53}\text{Ga}_{0.47}\text{As}$ (150 nm) at 680 °C, followed by $\text{In}_{0.52}\text{Al}_{0.48}\text{As}$, $\text{In}(\text{Al}_{0.6}\text{Ga}_{0.4})\text{As}$, $\text{In}(\text{Al}_{0.25}\text{Ga}_{0.75})\text{As}$, and $\text{In}_{0.53}\text{Ga}_{0.47}\text{As}$ (150 nm each) at 720 °C, and $\text{In}_{0.52}\text{Al}_{0.48}\text{As}$ (150 nm) and an InP layer cap layer (100 nm) at 760 °C. The SIMS profile of O, C, Si, and H atoms of this structure with Al marker is illustrated in Fig. 3. The O concentration in $\text{In}_{0.52}\text{Al}_{0.48}\text{As}$ at 720 °C is $\sim 2 \times 10^{16} \text{ cm}^{-3}$, which is significantly lower than that at 680 °C. Further increase in the growth temperature does not affect O concentration significantly. The O concentration is also strongly dependent on the Al content of the layers at 680 °C and becomes less sensitive at higher temperature. For $\text{In}_{0.53}\text{Ga}_{0.47}\text{As}$ layers, there is no noticeable dependence of the O concentration on the growth temperature, with the O level being as low as $5 \times 10^{15} \text{ cm}^{-3}$, close to the detection limit. The C concentration is below $1 \times 10^{16} \text{ cm}^{-3}$ in all layers. The growth temperature of 720 °C is considered as the optimal temperature for the active region with good surface morphology, improved optical quality, and low impurity contamination.

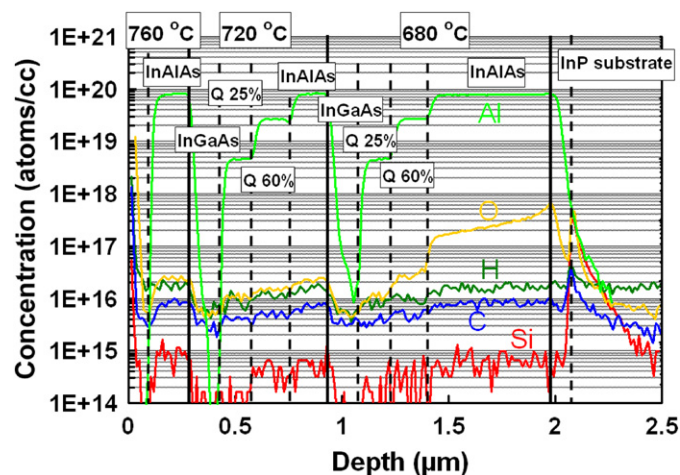


Fig. 3. SIMS profile of O, C, Si, and H atoms with Al marker in an InAlAs/In(Ga)As/InGaAs test structure grown at different temperatures.

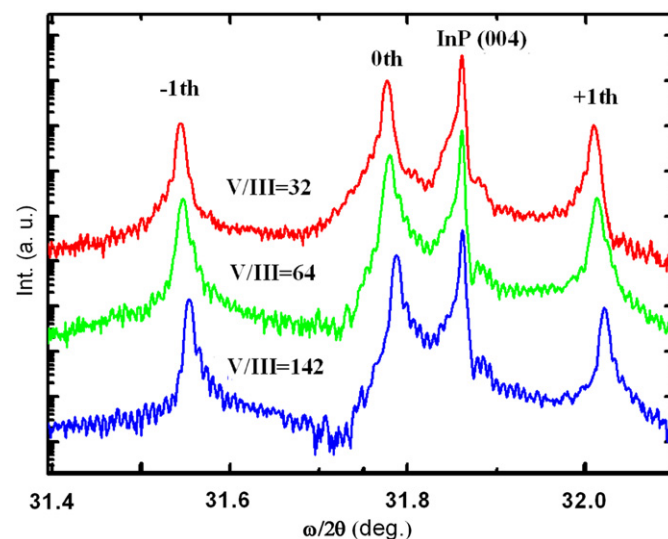


Fig. 5. XRD $\omega-2\theta$ scans measured near InP (0 0 4) for 30-period of $\text{In}_{0.58}\text{Ga}_{0.42}\text{As}/\text{In}_{0.52}\text{Al}_{0.48}\text{As}$ (8/15 nm) MQWs grown with different V/III ratios.

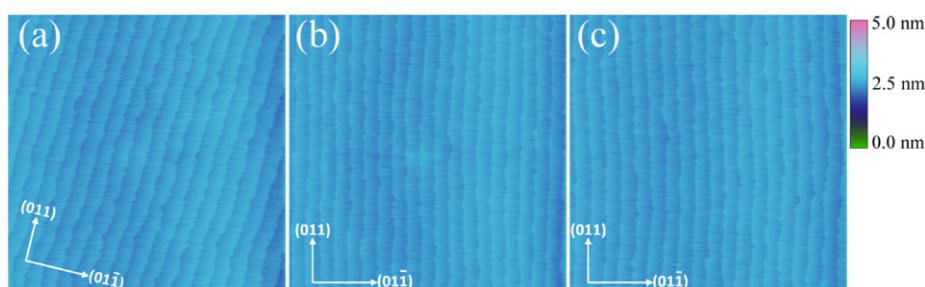


Fig. 4. AFM images ($10 \times 10 \mu\text{m}^2$) of 30-period of $\text{In}_{0.58}\text{Ga}_{0.42}\text{As}/\text{In}_{0.52}\text{Al}_{0.48}\text{As}$ (8/15 nm) MQWs grown with V/III ratios of (a) 32, (b) 64, and (c) 142 for InGaAs layer. The height scale is 5 nm for all images.

3.3. Effect of V/III ratios of InGaAs and InAlAs

After determining the optimal growth temperature for the InGaAs–InAlAs SL, the V/III ratios for growth of $\text{In}_{0.53}\text{Ga}_{0.47}\text{As}$ and $\text{In}_{0.52}\text{Al}_{0.48}\text{As}$ layers were investigated. Fig. 4 shows the AFM images of 30-period of $\text{In}_{0.58}\text{Ga}_{0.42}\text{As}/\text{In}_{0.52}\text{Al}_{0.48}\text{As}$ (8/15 nm) MQWs grown at 720 °C with V/III ratios of 32, 64, and 142 for InGaAs. The V/III ratio of the InAlAs layer was kept at 21. A slight compressive strain was added to the InGaAs QW to get a better XRD contrast. From Fig. 4, the stable step-flow dominates the growth at all V/III ratios and AFM does not reveal any noticeable change in the microscopic surface morphology. From the XRD $\omega-2\theta$ scans shown in Fig. 5, however, a higher V/III ratio seems to improve the interfacial quality of the MQW, as implied from the clearer thickness interference fringes between the satellite peaks. This may be attributed to the reduced In and Ga evaporation from the growing surface at higher V/III ratio of the InGaAs layers.

In contrast to the V/III ratio effect for InGaAs layer growth, the MQW surface morphology shows different behavior depending on the V/III ratio of the InAlAs layers. Fig. 6 shows the AFM images of 100-period of $\text{In}_{0.53}\text{Ga}_{0.47}\text{As}/\text{In}_{0.52}\text{Al}_{0.48}\text{As}$ (5/5 nm) MQWs grown with V/III ratios of 5, 21, and 84 for InAlAs. The V/III ratio of the InGaAs layer was kept at 116. At a V/III ratio of 84 shown in Fig. 6(c), the surface is relatively rough with dense nucleus on the terrace after 1- μm -thick MQW growth. A smaller V/III ratio in Fig. 6(b) allows for step-flow growth due to the enhanced surface mobility of adatoms. However, at a V/III ratio of 5 in Fig. 6(a), some pits were observed, as indicated by the arrow. To minimize the possible AsH_3 carry-over effect, a slightly lower V/III ratio in InGaAs may need to be used. Combined with the previous study, it is concluded that the optimal V/III ratios are ~ 120 for InGaAs and ~ 20 for InAlAs during the MQW growth at 720 °C.

3.4. Growth and characterization of the QCL

A QCL structure was grown employing the optimized growth conditions. The active region of the sample is based on a four-QW double-phonon resonance design similar to that reported in Ref. [6] except for the doping in the injector and is composed of 35 stages of the following sequence of lattice-matched $\text{In}_{0.53}\text{Ga}_{0.47}\text{As}/\text{In}_{0.52}\text{Al}_{0.48}\text{As}$ layers: 34/14/33/13/32/15/31/19/30/23/29/25/29/40/19/7/58/9/57/9/50/22 Å, where InAlAs layers are in bold and underlined layers are doped with $n \sim 6 \times 10^{16} \text{ cm}^{-3}$. The active region is sandwiched symmetrically by two $\text{In}_{0.53}\text{Ga}_{0.47}\text{As}$ waveguide layers (0.52 μm each, $n \sim 3 \times 10^{16} \text{ cm}^{-3}$), two InP cladding layers (3.5 μm each, $n \sim 1 \times 10^{17} \text{ cm}^{-3}$), and two InP plasmon-confinement layers (0.5 μm each, $n \sim 5 \times 10^{18} \text{ cm}^{-3}$). The structure is concluded by a 20 nm InGaAs n^+ cap layer. A 30 nm step-graded InGaAsP is inserted between the InGaAs waveguide and InP cladding layer to reduce the series resistance. The total thickness of the epitaxial structure is $\sim 11.3 \mu\text{m}$.

The QCL was grown at our optimized temperature of 720 °C, which is higher than the MOCVD QCL growth temperature reported in the literature [14,15]. The growth rate was $\sim 0.15 \text{ nm/s}$ for the

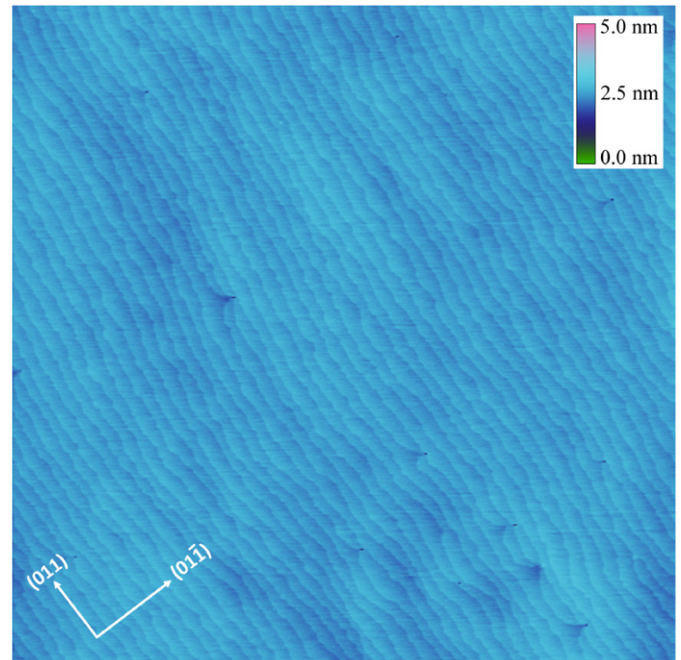


Fig. 7. AFM image ($10 \times 10 \mu\text{m}^2$) of the QCL epitaxial structure. The height scale is 5 nm.

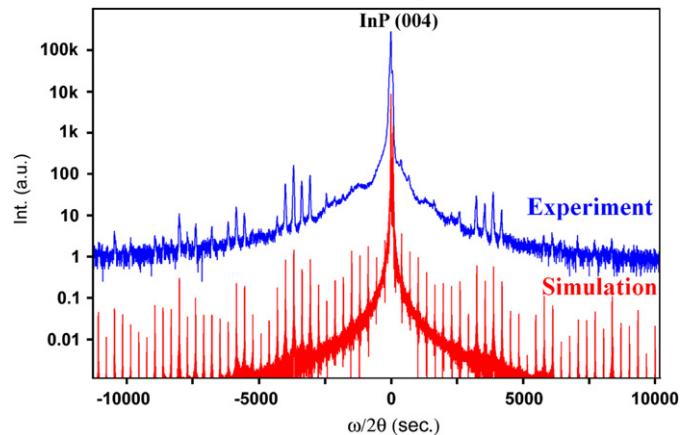


Fig. 8. XRD $\omega-2\theta$ scan measured near InP (0 0 4) diffraction condition (blue, top) and the simulated curve (red, bottom) of the QCL epitaxial structure. (For interpretation of the references to color in this figure legend, the reader is referred to the web version of this article.)

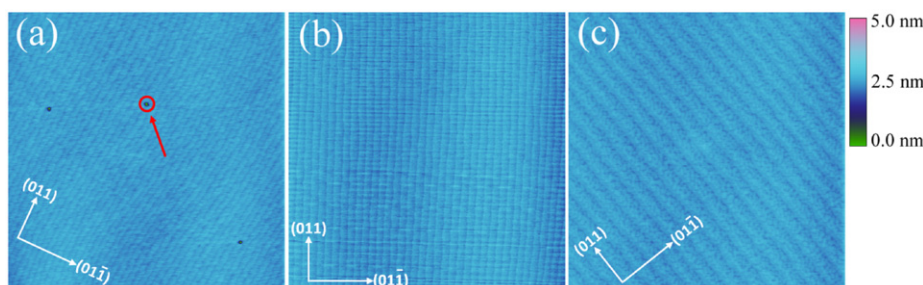


Fig. 6. AFM images ($10 \times 10 \mu\text{m}^2$) of 100-period of $\text{In}_{0.53}\text{Ga}_{0.47}\text{As}/\text{In}_{0.52}\text{Al}_{0.48}\text{As}$ (5/5 nm) MQWs grown at V/III ratios of (a) 5, (b) 21, and (c) 84 for InAlAs layer. The height scale is 5 nm for all images.

active region and ~ 0.48 nm/s for the waveguide and cladding layers. A 3-second growth interruption with group V overpressure was employed at each interface.

The sample surface was specular after growth with few visible defects. Fig. 7 shows the AFM image of the QCL wafer. Excellent surface morphology was obtained with a root-mean-square (RMS) roughness of only ~ 0.09 nm for $10 \times 10 \mu\text{m}^2$ scanning area. The XRD $\omega-2\theta$ scans and corresponding simulation of the QCL epitaxial structures are displayed in Fig. 8. A very small overall strain of the active region was recorded, with the separation between the SL zeroth-order peak and InP (0 0 4) being 59 arcsec. The FWHM of the zeroth order peak is only 42 arcsec. Satellite peaks are clearly visible. The measured periodicity of the QCL stage from the spacing of the satellite peaks is 59.3 nm, very close to the nominal value of 59.8 nm. Fig. 9 is the bright-field TEM images of the core active region and one magnified QCL stage containing an injector and an active region. Abrupt interfaces and uniform SL thickness along the growth direction were observed, indicating good structural quality and uniformity of the QCL wafer.

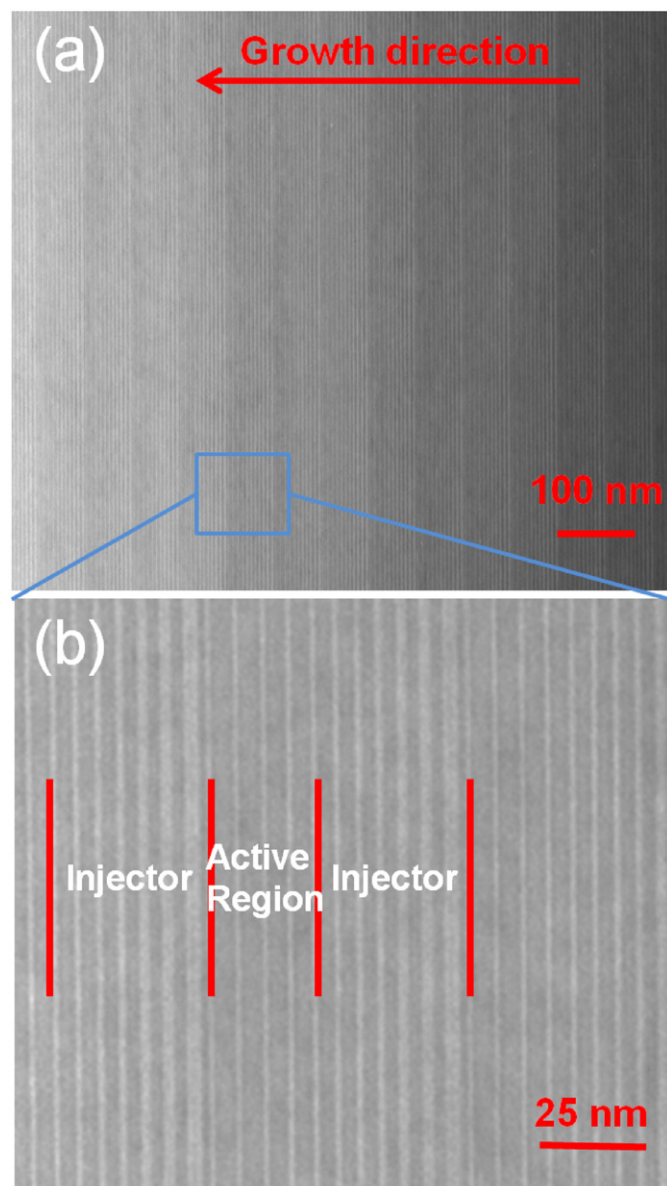


Fig. 9. TEM bright-field images of (a) part of the 35-stage core active region and (b) one of the cascade stage. The InGaAs layers are dark and InAlAs layers are bright.

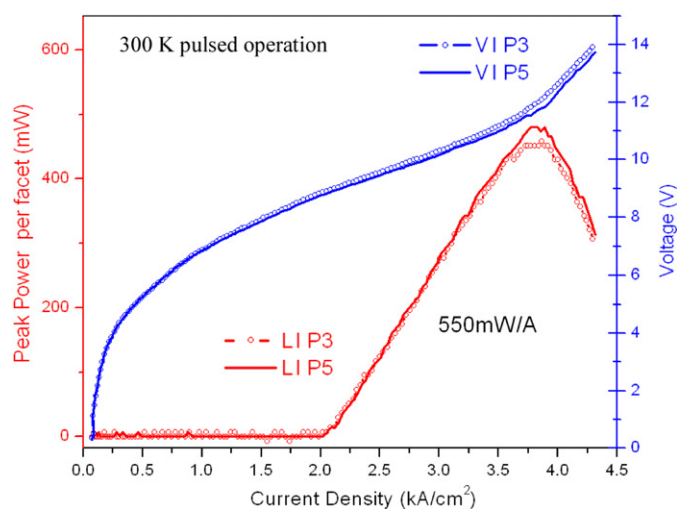


Fig. 10. Light output-voltage-current characteristics ($L-I$ and $V-I$ curves) for QCLs.

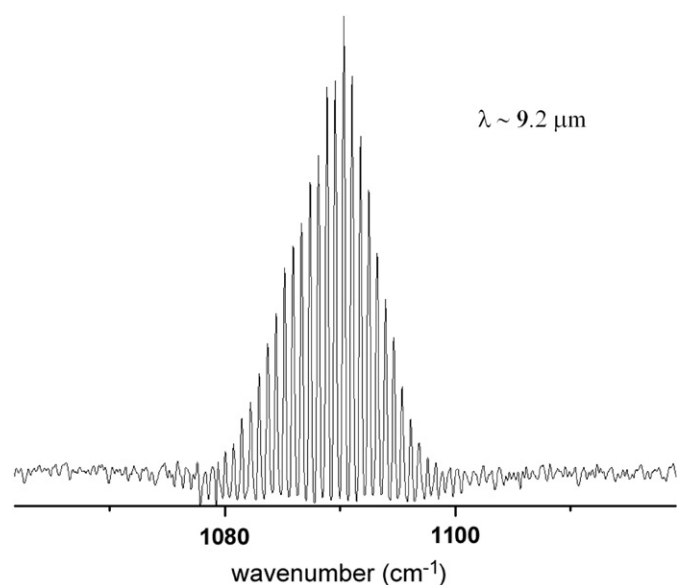


Fig. 11. Optical spectrum of the QCL.

The wafer was processed into 27.5- μm -wide 2-mm-long ridge structure lasers. Fig. 10 shows the light intensity and voltage versus current density ($L-I$ and $V-I$) characteristics of two devices (P3 and P5) measured at room temperature. Both of them exhibit similar device performance, with a threshold current density of $J_{\text{th}} \sim 2.0$ kA/cm² and a threshold voltage of ~ 9.1 V. The slope efficiency is ~ 550 mW/A and the maximum peak power is 480 mW. As indicated in Fig. 11, the emission wavelength of the laser is $\lambda \sim 9.2$ μm , close to the designed 9.3 μm . These data represent a comparable results to that of the QCLs with a similar design grown by either MBE or MOCVD [6,14,27].

4. Conclusions

Stable step-flow growth and low O and C concentrations have been achieved in InGaAs/InAlAs/InP heterostructures and QCLs through optimization of the key growth parameters in MOCVD. It was found that the misorientation of InP substrates plays a critical

role in dictating the InP surface morphology and the optimal off-cut angle is determined to be $\sim 0.06^\circ$, where step-bunching or hillock formation were completely eliminated. InGaAs/InAlAs MQW structures exhibit a stable step-flow growth at the temperature of 720°C and a V/III ratio of 116 for InGaAs and 21 for InAlAs. As revealed by SIMS, the O and C concentrations in InAlAs layers is only 2×10^{16} and $7 \times 10^{15} \text{ cm}^{-3}$, respectively. When applying these optimized conditions to a 35-stage QCL growth, step-flow surface, abrupt interfaces, low strain, and precise periodicity were obtained, indicating an excellent capability of MOCVD in controlling the interface, thickness, composition, and morphology of complicated structures. After processed into ridge waveguide laser, the QCL demonstrates a threshold current density of 2.0 kA/cm^2 and a slope efficiency of $\sim 550 \text{ mW/A}$ at room temperature in pulsed mode.

Acknowledgements

This work was performed in part at the Center for Nanoscale Systems (CNS), a member of the National Nanotechnology Infrastructure Network (NNIN), which is supported by the National Science Foundation under NSF award no. ECS-0335765. CNS is part of the Faculty of Arts and Sciences at Harvard University. Authors would like to acknowledge useful technical discussions with Dr. Christine Wang of MIT Lincoln Lab. One of the authors (R.D.D) acknowledges the support of the Steve W. Chaddick Endowed Chair in Electro-Optics and The Georgia Research Alliance.

References

- [1] R.F. Kazarinov, R.A. Suris, *Fiz. Tek. Poluprov.* 5 (1971) 797.
- [2] O. Cathabard, R. Teissier, J. Devenson, J.C. Moreno, A.N. Baranov, *Appl. Phys. Lett.* 96 (2010) 141110.
- [3] R. Köhler, A. Tredicucci, F. Beltram, H.E. Beere, E.H. Linfield, A.G. Davies, D.A. Ritchie, R.C. Iotti, F. Rossi, *Nature* 417 (2002) 156.
- [4] J. Faist, F. Capasso, D.L. Sivco, C. Sirtori, A.L. Hutchinson, A.Y. Cho, *Science* 264 (1994) 553.
- [5] G. Strasser, S. Gianordoli, L. Hvozdar, W. Schrenk, K. Unterrainer, E. Gornik, *Appl. Phys. Lett.* 75 (1999) 1345.
- [6] D. Hofstetter, M. Beck, T. Aellen, J. Faist, U. Oesterle, M. Illegems, E. Gini, H. Melchior, *Appl. Phys. Lett.* 78 (2001) 1964.
- [7] R. Maulini, M. Beck, J. Faist, E. Gini, *Appl. Phys. Lett.* 84 (2004) 1659.
- [8] A. Lyakh, C. Pflügl, L. Diehl, Q.J. Wang, F. Capasso, X.J. Wang, J.Y. Fan, T. Tanbun-Ek, R. Maulini, A. Tsekoun, R. Go, C. Kumar, N. Patel, *Appl. Phys. Lett.* 92 (2008) 111110.
- [9] Y. Bai, S. Slivken, S.R. Darvish, M. Razeghi, *Appl. Phys. Lett.* 93 (2008) 021103.
- [10] A. Lyakh, R. Maulini, A. Tsekoun, R. Go, C. Pflügl, L. Diehl, Q.J. Wang, F. Capasso, C. Kumar, N. Patel, *Appl. Phys. Lett.* 95 (2009) 141113.
- [11] R. Maulini, A. Lyakh, A. Tsekoun, R. Go, C. Pflügl, L. Diehl, F. Capasso, C. Kumar, N. Patel, *Appl. Phys. Lett.* 95 (2009) 151112.
- [12] P.Q. Liu, A.J. Hoffman, M.D. Escarra, K.J. Franz, J.B. Khurgin, Y. Dikmelik, X. Wang, J.-Y. Fan, C.F. Gmachl, *Nat. Photon.* 4 (2010) 95.
- [13] Y. Bai, S. Slivken, S. Kuboya, S.R. Darvish, M. Razeghi, *Nat. Photon.* 4 (2010) 99.
- [14] A.B. Krysa, J.S. Roberts, R.P. Green, L.R. Wilson, H. Page, M. Garcia, J.W. Cockburn, *J. Cryst. Growth* 272 (2004) 682.
- [15] D. Bour, M. Troccoli, F. Capasso, S. Corzine, A. Tandon, D. Mars, G. Höfler, *J. Cryst. Growth* 272 (2004) 526.
- [16] C.A. Wang, R.K. Huang, A. Goyal, J.P. Donnelly, D.R. Calawa, S.G. Cann, F. O'Donnell, J.J. Plant, L.J. Missaggia, G.W. Turner, A. Sanchez-Rubio, *J. Cryst. Growth* 310 (2008) 5191.
- [17] C.A. Wang, A. Goyal, R. Huang, J. Donnelly, D. Calawa, G. Turner, A. Sanchez-Rubio, A. Hsu, Q. Hu, B. Williams, *J. Cryst. Growth* 312 (2010) 1157.
- [18] J.S. Roberts, R.P. Green, L.R. Wilson, E.A. Zibik, D.G. Revin, J.W. Cockburn, R.J. Airey, *Appl. Phys. Lett.* 82 (2003) 4221.
- [19] M. Troccoli, L. Diehl, D.P. Bour, S.W. Corzine, N. Yu, C.Y. Wang, M.A. Belkin, G. Höfler, R. Lewicki, G. Wysocki, F.K. Tittel, F. Capasso, *IEEE J. Lightwave Technol.* 26 (2008) 3534.
- [20] Precursors are provide by SAFC Hitech (formerly Epichem), Haverhill, MA.
- [21] M. Shinohara, N. Inoue, *Appl. Phys. Lett.* 66 (1995) 1936.
- [22] H. Dumont, Y. Monteil, J. Bouix, *Appl. Surf. Sci.* 161 (2000) 286.
- [23] R.J. Young, L.O. Mereni, N. Petkov, G.R. Knight, V. Dimastrodonato, P.K. Hurley, G. Hughes, E. Pelucchi, *J. Cryst. Growth* 312 (2010) 1546.
- [24] J.G. Cederberg, M.E. Overberg, *J. Cryst. Growth*, in press, doi:10.1016/j.crysgro.2010.08.040.
- [25] M.I. Amanti, G. Scalari, R. Terazzi, M. Fischer, M. Beck, J. Faist, A. Rudra, P. Gallo, E. Kapon, *New J. Phys.* 11 (2009) 125022.
- [26] G.B. Stringfellow, *Organometallic Vapor-Phase Epitaxy: Theory and Practice*, 2nd Edition, Academic Press, New York, 1999.
- [27] C. Pflügl, L. Diehl, A. Tsekoun, R. Go, C.K.N. Patel, X. Wang, J. Fan, T. Tanbun-Ek, F. Capasso, *Electron. Lett.* 43 (2007) 1026.